Materials Science in Semiconductor Processing 77 (2018) 50–57

Contents lists available at ScienceDirect

Materials Science in Semiconductor Processing

journal homepage: www.elsevier.com/locate/mssp

Sol-gel grown aluminum/gallium co-doped ZnO nanostructures: Hydrogen gas sensing attributes

Hayder J. Al-Asedy[a,b,c], Noriah Bidin[a,*], Shuruq A. Al-khafaji[d], Hazri Bakhtiar[a]

[a] Universiti Teknologi Malaysia, Laser Center, Ibnu Sina Institute for Scientific and Industrial Research, Johor Bahru, Johor 81310, Malaysia
[b] Universiti Teknologi Malaysia, Department of Physics, Faculty of Science, Johor Bahru, Johor 81310, Malaysia
[c] University of Al-Qadisiyah, Faculty of Education, Physics Department, Diwaniyah, Iraq
[d] University of Al-Qadisiyah, Faculty of Engineering, Roads and Transports Department, Diwaniyah, Iraq

ARTICLE INFO

Keywords:
Nanostructures
Co-doping
Sol-gel
Resistivity
Hydrogen gas sensor

ABSTRACT

Aluminum (Al) and Gallium (Ga) co-doped ZnO nanostructures (AGZO NSs) were prepared on p-type Si(100) substrate using sol-gel united spin coating method. Ga contents were varied from 1 to 5 at% at fixed Al doping (1 at%). Synthesized samples were annealed at 500 °C for 3 h. The structural, morphological, and electrical property of the optimum sample (containing 3 at% of Ga) were determined. Optimum AGZO NSs enclosing highest density of nanorod (NR) arrays were selected to fabricate a hydrogen gas (H_2) sensor. As-grown AGZO NSs revealed hexagonal wurtzite structure with mean grain size ≈ 41.20 nm and resistivity ≈ 0.6475×10^{-2} Ω cm. The gas sensing attributes of the developed sensor was evaluated for two different temperatures (at 100 and 150 °C) under varying gas H_2 contents (from 250 to 1750 ppm). Furthermore, the selectivity of the AGZO NSs for three different gases such as H_2, CO and CH_4 were examined. The sensitivity of the sensor at 100 °C was augmented sharply from 60% to 385% with the increment of H_2 gas contents from 250 to 1750 ppm. This enhancement was attributed to the increases of hydrogen gas current (I_H) and good stability of the air atmosphere. The synthesized AGZO NSs have high potential for gas sensing, photovoltaic and field emission applications.

1. Introduction

Transparent metal oxide semiconductor nanostructures (NSs) became popular due to their exceptional chemical and physical properties. Transparent conducting oxide (TCO) thin films have been extensively studied and applied for various purposes as gas sensors, light emitting diodes (LEDs), transistors and solar cells [1]. Among all the direct bandgap semiconductors NSs, Zinc Oxide (ZnO) NS is greatly demanding due to its wide bandgap (≈ 3.37 eV) and large exciton binding energy (≈ 60 eV). ZnO is n-type intrinsic semiconductor due to the presence of native defects of Zn interstitials and oxygen vacancies that act as majority carriers (donor). In pertaining high efficient solar cells, transparent conducting electrodes required to have minimum resistance and maximum transmittance. Although indium tin oxide (ITO) is presently leading the transparent electrode with highest performance but its application is limited. This is subjected to its highly toxicity, low stability and high cost. Therefore, to resolve such drawbacks, alternative TCO needs to be considered.

It is well known that the optical and electrical properties of ZnO can be improved by doping it with elements of group III such as trivalent Al and Ga. Replacement of Zn atoms in the parent crystal structure via trivalent elements has been performed to modify the ZnO lattice to achieve ITO equivalent improved performance [2]. In the past, diverse techniques were developed to produce good quality doped ZnO films. These methods include chemical vapor deposition (CVD) [3], spray pyrolysis [4], magnetron sputtering [5], pulsed laser ablation [6], plasma-assisted molecular beam epitaxy [7], and sol-gel [8]. Among all, sol-gel technique was found to be beneficial due to its low cost, accuracy, easy processing, consistency, flexibility, wide area coating ability, and less time consumption. Besides, sol-gel synthesized materials showed high crystallinity and excellent NSs morphology [9].

Some related studies based on Al and Ga co-doped ZnO NSs film to modify their optical and electrical properties have been carried by Zhu et al., [10]. It was elucidated that significantly lower ionic radius of Al^{+3} (r_{Al} = 0.054 nm) compared to Zn^{+2} (r_{Zn} = 0.74 nm) is a major factor that responsible for the lattice deformation in Al substituted ZnO matrix (AZO film). Although the ionic radius of Ga (r_{Ga} = 0.062 nm) [11] is slightly greater than Al but the extent of lattice mismatch is less significant with Zn. Literature revealed that an additional doping of Ga in AZO structure could improve the optical and electrical attributes.

* Corresponding author.
E-mail address: noriah@utm.my (N. Bidin).

https://doi.org/10.1016/j.mssp.2018.01.011
Received 11 August 2017; Received in revised form 2 January 2018; Accepted 13 January 2018

Moreover, the effects of changing Al and Ga doping concentration on the ZnO thin films are still lacking [12]. Mamat et al., [13] deposited Al doped ZnO thin films on microscope glass substrate using sol-gel combined spin-coating method. Ebrahimifard et al., [11] had prepared AGZO thin films using the same method. Vishwas et al., [14] synthesized polycrystalline (hexagonal phase) Al doped ZnO NSs at deposition temperature of 400 °C.

Despite many efforts to produce trivalent metals doped ZnO nanofilm a reproducible method for solution preparation with controlled growth conditions are still deficient. The data on the influence of solution molarity, types of dopants and contents, heat treatment temperature and time, ageing time, substrate types, annealing temperature and time, and deposition speed and time on the growth morphology of such NSs are still inadequate. Moreover, the validity and the reproducibility of the results on the improvement of structural, physical, morphological, optical, gas sensing, and electrical properties reported by various researchers remain debatable. Very few studies compared the diverse properties of AZO and GZO films that were grown under identical conditions. Lee et al., [15] assessed the effects of annealing on the electronic and optical characteristics of AGZO thin films and achieved a resistivity as low as $4.5 \times 10^{-2}\ \Omega$ cm at an annealing temperature of 450 °C. X-ray photoelectron spectral analysis revealed a Fermi-level shift $\approx$ 0.6 eV and the optical bandgap was widened by an amount $\approx$ 0.3 eV.

In the absence of oxygen atmosphere and at room temperature, Kim et al., [16] synthesized AGZO thin films on fused quartz (FQ) and Cyclo-olefin Polymer (COP) substrates using radio frequency magnetron sputtering technique. The elemental distributions of Al, Ga, Zn and O were observed all over the film without any compositional change at working pressure. The resistivity of AGZO/FQ and AGZO/COP films were varied in the range of 0.03–4.07 Ω cm and 0.04–5.73 Ω cm, respectively. Meanwhile, a transmittance above 85% was obtained via the appropriate control of the working pressure. Using inexpensive sol-gel united spin coating method, Serrao et al. [17] prepared some transparent conducting ZnO films on the glass substrate by Al and Ga doping as well as Al/Ga (1:1) co-doping. Such thin films displayed very low resistivity ($2.54 \times 10^{-3}\ \Omega$ cm) and high visible transmittance (above 83%).

Considering the importance of Al/Ga co-doped ZnO NSs based films, AGZO films were deposited on Si substrate via sol-gel mediated spin-coating method. As-synthesized AGZO films containing aligned vertically nanorods were characterized. Furthermore, a H_2 gas sensor was fabricated using the best sample to determine its effective gas sensing property.

2. Experimental

Al/Ga co-doped ZnO (AGZO) films were grown by using analytical grade (Alfa Aesar, purity 99.999%) chemical compounds of zinc acetate dehydrate ($Zn(CH_3COO)_2{\cdot}2H_2O$), aluminum nitrate nonahydrate ($Al(NO_3)_3{\cdot}9H_2O$), gallium nitrate nonahydrate ($Ga(NO_3)_3{\cdot}9H_2O$), 2-propanol and ethanolamine. Initially, $Al(NO_3)_3{\cdot}9H_2O$ was dissolved at room temperature in a solution made from 2-propanol and ethanolamine. The concentration of $Zn(CH_3COO)_2{\cdot}2H_2O$ was 0.1 M and the molar ratio of ethanolamine to zinc acetate was 1:1. The solution was magnetically stirred constantly for 30 min to get a homogeneous and clear mixture. Later, the resulting ZnO solution was doped with Al (1 at %) and Ga (3 at%). Next, the mixture was dissolved in methanol at 60 °C for 90 min and stirred continuously to obtain a transparent solution. Then, few drops of the solution were poured on a p-type Si(100) substrate before being spin coated for a duration of 30 s at the angular speed of 3000 rpm which was repeated for 10 times. The achieved uniform AGZO film was further dried for 20 min at 300 °C. Finally, the dried solid film was annealed for 3 h at 500 °C in atmospheric pressure.

The crystalline structure of as-synthesized sample was determined using X-ray diffraction (XRD, Bruker D8 Advance Diffractometer operated at 40 kV and 100 mA) analysis with Cu-Kα_1 radiations of wavelength 1.5406 Å in the scanning range 2θ = 20–80°. A slow speed of scanning $\approx$ 1.2°/min with a resolution of 0.01° was used. Elemental composition and surface morphology of the sample were analyzed using energy dispersive X-ray (EDX) spectroscopy and field emission scanning electron microscopy (FESEM, ZEISS SUPRA 35 VP), respectively. Four-point probe method was used to measure the resistivity of the annealed AGZO NSs sample.

The optimum AGZO NSs sample (3 at% of Ga) was used to design a hydrogen (H_2) gas sensor. A thin layer (thickness $\approx$ 250 nm) of silver (Ag) was deposited above the AGZO film via vacuum thermal evaporation method. Two planar Ag electrodes with a gap area of 2 cm × 2 cm were fabricated on the top of the AGZO film. The H_2 gas sensing performance of the designed sensor was measured using a self-designed test system adopted from previous researcher [18]. The temperature of the film-based sensor was varied from 100 to 150 °C using a heater made of Ni–Cr coil. A thermocouple was placed on the film surface to record the temperature. The concentrations of the inserted target H_2 gas within the glass chamber were varied (250, 500, 1250 and 1750 ppm) under a constant air flow rate. A high mega-ohm multi-meter was interfaced with a computer to measure the resistance of the AGZO NSs.

3. Results and discussion

Fig. 1 illustrates the XRD pattern of the optimum AGZO sample annealed at 500 °C in the air for 3 h duration. The observed XRD peaks were indicated to the hexagonal wurtzite structure of ZnO, which tallied from JCPDS Card No. 36-1451. The occurrences of sharp peaks at 2θ = 31.86°, 34.42°, 36.28°, 47.68°, 56.53°, 62.92° and 66.36° were assigned to Bragg's reflections from (100), (002), (101), (102), (110), (103) and (200) lattice planes. Secondary phases such as Al_2O_3, Ga_2O_3, $ZnAl_2O_4$ or $ZnGa_2O_4$ as well as the impurities were completely absent in the synthesized AGZO film. The appearance of most intense peak indicated the preferential growth of nanocrystallite (hexagonal wurtzite crystal structures) along the (101) lattice direction (crystallographic c-axis) which was consistent with earlier finding [19]. The emergence of intense peaks corresponding to the growth orientation along (100), (002), and (101) lattice planes were matched with the JCPDS 36-1451 standard. The preferred growth along (101) lattice direction compared to other crystallographic orientations was attributed to the lower surface energy of (101) plane [20].

The sharpness of the XRD peak indicated the good crystallinity of AGZO NSs and the associated broadening of the peak signified the quantum size effects of nanocrystallites. Most of the physical deposition methods for the synthesis of Al-doped ZnO film suffer from extrinsic residual stress generation in the film. The size of nanocrystallites (grain

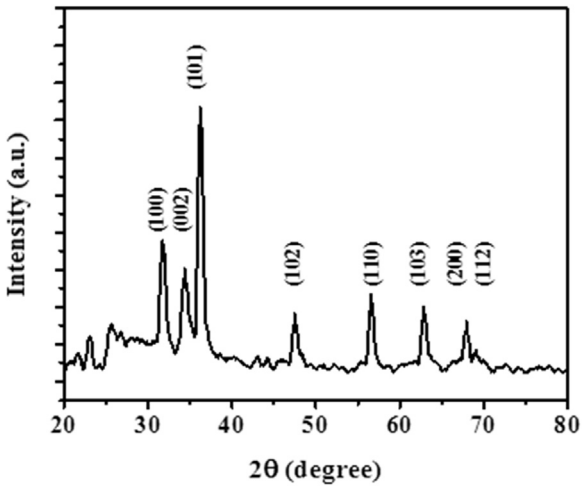

Fig. 1. XRD pattern of optimum AGZO NSs based film annealed in air at 500 °C for 3 h.

Table 1
The FWHM, D (nm), lattice constants, volume, density, the resistivity, carrier concentration and Hall mobility of the optimum AGZO film.

D (nm)	FWHM for (101)	a (Å)	c (Å)	c/a	V (Å)$^{-3}$	d (gm cm^{-3})	ρ ($\times 10^{-2}$) (Ω cm)	Carrier conc.($\times 10^{19}$) cm^{-3}	Hall mobility (cm^2/V s)
41.20	0.349	3.249	5.208	1.602	47.608	5.657	0.647	1.239	7.667

diameter) D, was calculated using Scherrer's formula, whereby the intense XRD peak was considered [21]:

$$D = \frac{k.\lambda}{\beta\cos\theta} \quad (1)$$

where k is the shape factor taken as 0.9, λ is the wavelength of X-ray, β is the FWHM value and θ is the XRD peak position.

Table 1 enlists the estimated values of mean crystallite diameter (D in nm), FWHM, lattice constants (a and c). The estimated nanocrystallite sizes in the present case appeared to be much smaller than those reported earlier (64 nm and 280 nm) [22]. The gradual increase in the average crystallite size indicated an improvement in the crystallinity. Conversely, rapid increases in the nanocrystallite sizes signified the development of multi-domains in the AGZO NSs. The observed alteration in the stoichiometric ratio of Zn to O and the improved nanocrystallinity was ascribed to the effect of co-doping the AZO film with Ga [23]. Moreover, the lowering of the polycrystallinity of AZO film due to Ga co-doping was clearly reflected in the increased of FWHM. The values of lattice parameters (a and c) of hexagonal wurtzite structure were calculated from the XRD peak via the relation [24]:

$$a = \frac{\lambda}{\sqrt{3}\sin\theta_{100}}, \quad c = \frac{\lambda}{\sin\theta_{002}} \quad (2)$$

Values of a and c were estimated to be 3.249 Å and 5.208 Å, respectively with $\frac{c}{a} \approx 1.602$. The crystalline density (d) and the volume (V) of the hexagonal unit cell was calculated (Table 1) using [25]:

$$d = \frac{1.6609 \cdot M \cdot n}{V}, V = 0.866 \quad a^2 \cdot c \quad (3)$$

where M is the molecular weight of the substance and n is the number of formula units in the unit cell ($n = 2$ for ZnO).

Fig. 2 shows the FESEM image of the optimum AGZO film which consisted of granular porous morphology. The enhanced crystallinity of the NSs implied a favorable crystallization due to the co-doping of extra Ga into the AZO film. Besides, inclusion of Ga appreciably modified the surface morphology where more aligned irregular hexagonal AGZO nanorods were emerged. Estimated diameters of these aligned nanorods were ranged from 43 to 58 nm with average length ≈ 337 nm. The ionic radius inequality between Ga^{3+} (0.062 nm), Al^{3+} (0.054 nm) and Zn^{2+} (0.074 nm) in the lattice site of ZnO played a decisive role in the overall surface morphology modification of the studied AGZO films. The magnified images of the AGZO film grown at 90 °C for 3 h duration revealed inclined nanorods in the angular range of 45–90° with respect to substrate. Thus, the top-view of the FESEM images displayed

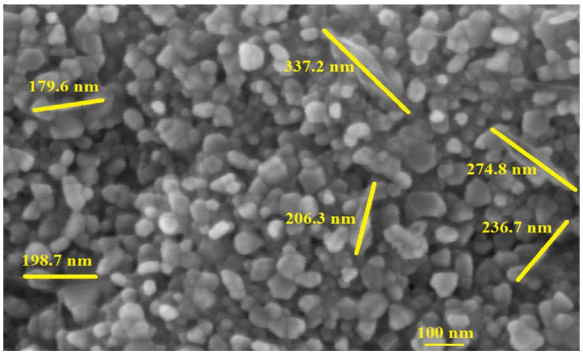

Fig. 2. Top view of FESEM image of AGZO film reveling NSs morphology.

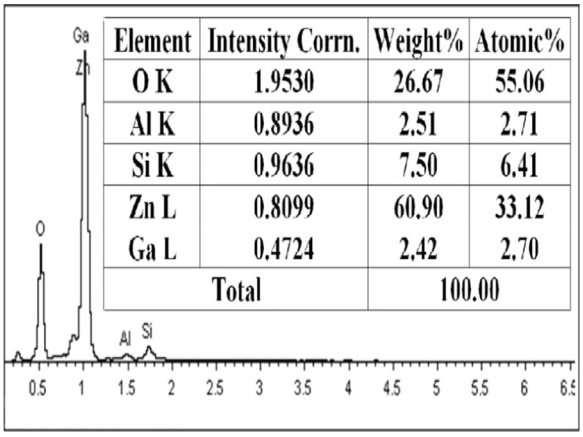

Element	Intensity Corrn.	Weight%	Atomic%
O K	1.9530	26.67	55.06
Al K	0.8936	2.51	2.71
Si K	0.9636	7.50	6.41
Zn L	0.8099	60.90	33.12
Ga L	0.4724	2.42	2.70
Total		100.00	

Fig. 3. EDX spectra of optimum AGZO film.

partially oblique nature of the nanorod tips. Although the nanorods tips were adjacent to each other but most of the nanorods were in contact and soldered together at several points during the AGZO film growth. The lengths and average diameters of all the vertical (longitudinal) NRs were convergent. However, for lateral NRs only the lengths were convergent. ImageJ software was used to calculate the lengths and diameters of these NRs.

Fig. 3 shows the EDX spectra of the AGZO film in the presence of appropriate elements. Experimentally detected atomic and weight percentages of elements were well matched with the calculated one as demonstrated in the inset. Table 1 summarizes the measured electrical properties including the resistivity, the Hall mobility and the carrier concentration. Four-point probe method was used to measure the electrical resistivity. The resistivity of the AGZO film was low (≈ 0.647 × 10^{-2} Ω cm) [26] and the Hall mobility was high (≈ 7.667 cm^2 V^{-1} s^{-1}) [26]. This lowering in the resistivity and enhancement in the Hall mobility were primarily attributed to the large carrier concentration (1.239 × 10^{19} cm^{-3}) and improved crystallinity of the AGZO film due to Ga co-doping. Substitution of Zn^{+2} ions in the lattice sites by Ga^{+3} and Al^{+3} ions released extra electrons into the conduction band and thus increased the carrier concentration. The Ga^{+3} ions in the interstitial were responsible for the enhancement of AGZO film conductivity.

Hall mobility (μ_H) of the AGZO film was calculated based on electrical resistivity (ρ), electronic charge (e), and carrier concentration (N) using the following expression [27]:

$$\rho = \frac{1}{eN\mu_H} \quad (4)$$

It is important to note that an increase in the value of ρ as well as N could cause a drop in the Hall mobility. The observed enhancement in the Hall mobility was attributed to the significant improvement of the microstructure and complete elimination of the carrier scattering centers. Generally, the Hall mobility (μ_H) is based by the carrier scattering. The total Hall mobility in terms of ionized impurity scattering (μ_i), lattice vibration scattering (μ_l), and grain boundary scattering (μ_g) can be expressed as [28,29]:

$$\frac{1}{\mu_H} = \frac{1}{\mu_i} + \frac{1}{\mu_l} + \frac{1}{\mu_g} \quad (5)$$

The contribution of lattice vibration scattering is insignificant at

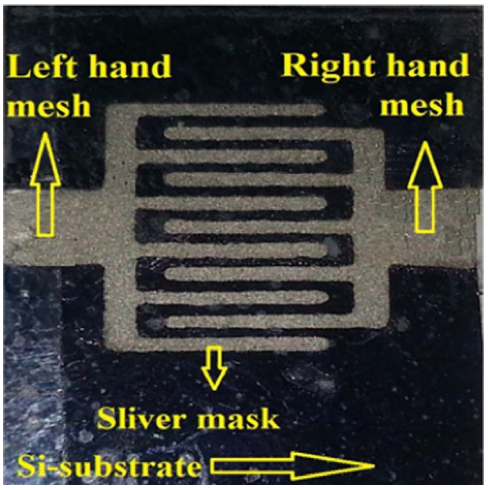

Fig. 4. Designed H_2 gas sensor using optimum AGZO nanofilm containing vertically aligned NSs.

room temperature and become predominant only at high temperature [28]. The grain boundary scattering involvement become considerable for polycrystalline semiconductor thin film [29] that includes high defect density at the grain boundary because of crystal imperfection from chemisorbed oxygen and various oxides segregation. The presence of these boundary defects is responsible for capturing the carriers, easy charging, and finally the formation of depletion layers that acts as potential barrier towards carrier transport. The involvement of grain boundary scattering is almost insignificant for crystallites having size much above the mean electronic free path [29]. The mean free path of carriers was calculated from $l = \frac{nh}{2\pi\mu e}$ [28] and found to be lower than 4 nm. This length was indeed much shorter than the average size of AGZO crystallite ($\approx$ 27 nm). Thus, the impurity scattering was regarded as the dominant factor.

Fig. 4. depicts the designed H_2 gas sensor using fabricated AGZO nanofilm. Meanwhile the performance of H_2 gas sensor based fabricated sensor of AZGO sample which adopted from other researcher [18] is shown in Fig. 5. The film surface was heated at 100 and 150 °C wherein the target H_2 gas at varying concentrations was injected into the sensing system under constant air flow rate. A high mega-ohm multimeter was used to record the resistance of the film. The response (***S***) of gas sensor was calculated using

$$S = \frac{(I_H - I_{air})}{I_{air}} \times 100\% \quad (6)$$

where I_{air} and I_H are the resistance of the sensor measured in the air and in the presence of target H_2 gas, respectively. Response time (T_{90}) is required by the target gas to attain 90% of the saturation resistance

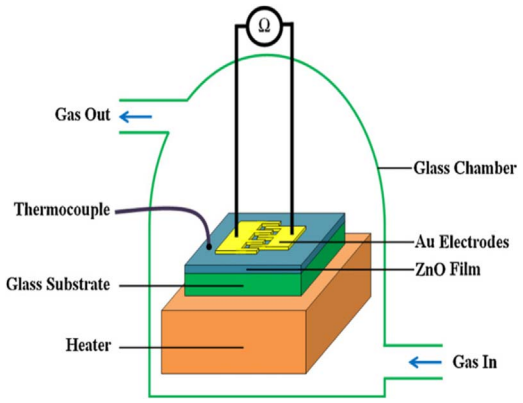

Fig. 5. Typical H_2 gas detection device enclosing the designed sensor.

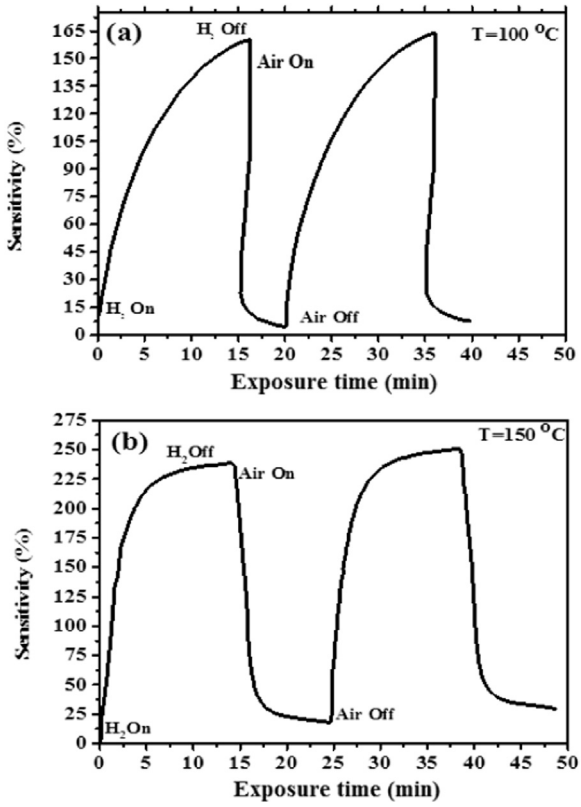

Fig. 6. Sensitivity and repeatability of the fabricated AGZO film sensor at different operation temperatures: (a) 100 °C and (b) 150 °C.

[30]. Thus, the rise and decay or recovery time of gas the sensor were measured. The rise and decay time are the time required to grow and decline the peak response by 90% and 10%, respectively [31].

Fig. 6(a) and (b) show the repeatability of sensitivity with respect to the exposure time of the fabricated AGZO film based sensor at 100 and 150 °C under the exposure of H_2 (1250 ppm) for 50 min. The sensitivity, response time, and recovery time of the ZnO NSs based sensor operated at 100 and 150 °C are enlisted in Table 2. The response time is slightly increases, the recovery time is elongated, and the sensitivity is improved with the increasing of operation temperature. The improvement in the surface activity of AGZO film based sensor with the increase of operating temperatures led to enhancement of the gas adsorption/desorption rate. In short, this improvement in the conductivity and sensitivity of the sensor at higher temperature was ascribed to the enhancement of atmospheric oxygen adsorption on the surface of ZnO NSs, thereby the liberation of large number of free electrons. Thus, upon exposing the ZnO NSs sensor to hydrogen gas (Fig. 7), large number trapped electrons were released from the adsorbed oxygen molecules on the ZnO surface which in turn enhanced the sensor's conductivity and sensitivity [32]. Good repeatability of the sensor is clearly demonstrated in Figs. 6 and 7.

Fig. 7 depicts the H_2 concentration (250, 500, 1250 and 1750 ppm) dependent response of AZGO NSs based sensor at the optimum operating temperature of 100 °C. The best sensitivity was achieved for a gas concentration of 1750 ppm. Moreover, the lowering in the sensitivity at

Table 2
Operating temperature dependent sensitivity, rise time and recovery time of the fabricated H_2 gas sensor.1.

Temperature (°C)	Sensitivity (%)	Rise time (min)	Recovery time (min)
100	141	10	8
150	214	6.5	5

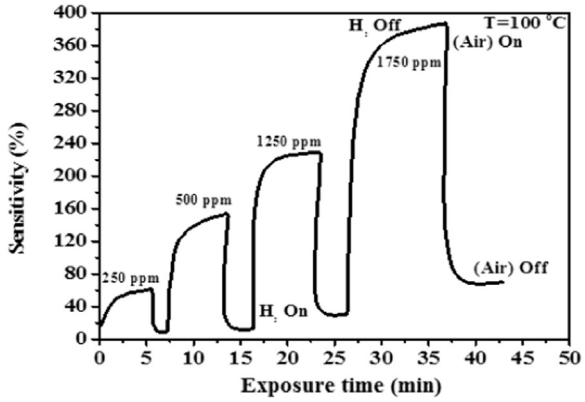

Fig. 7. Real-time sensitivity of the sensor at 100 °C with changing H_2 gas exposures (250, 500, 1000 and 1750 ppm).

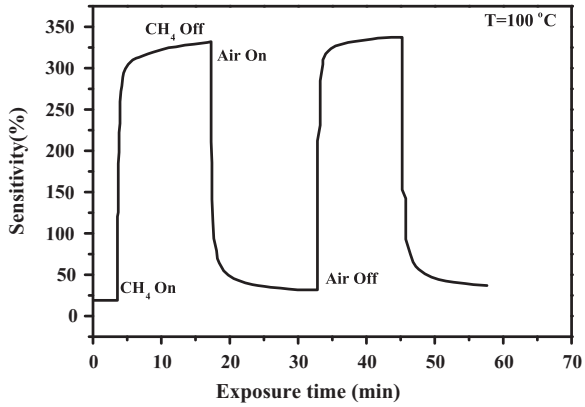

Fig. 8. Sensitivity and repeatability of the fabricated AGZO film sensor at operation temperature 100 °C for CH_4 gas.

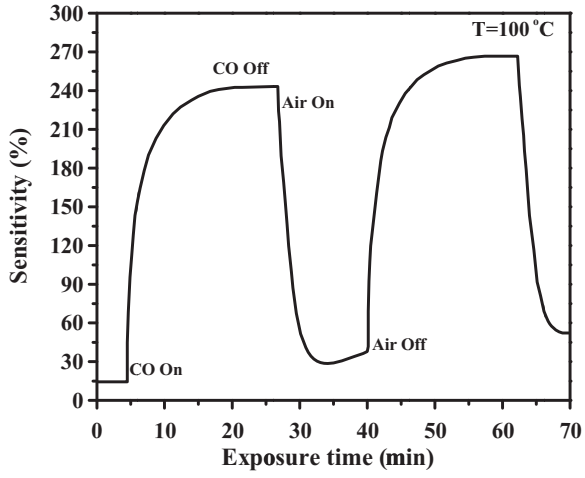

Fig. 9. Sensitivity and repeatability of the fabricated AGZO film sensor at operation temperature 100 °C for CO gas.

higher gas concentration was ascribed to the influence of surface states saturation. The sensitivity at 100 °C was sharply increased from 60% to 385% when the gas concentration was increased from 250 to 1750 ppm. Figs. 8 and 9 display the sensitivities and repeatability of the fabricated AGZO sensor for CO and CH_4 gases at operation temperature of 100 °C, respectively.

Fig. 10 presents a schematic diagram for the gas sensing mechanism of the AGZO NSs based sensor [33]. At the ambient temperature, the AGZO film surface adsorbed oxygen (O_2) molecules from the

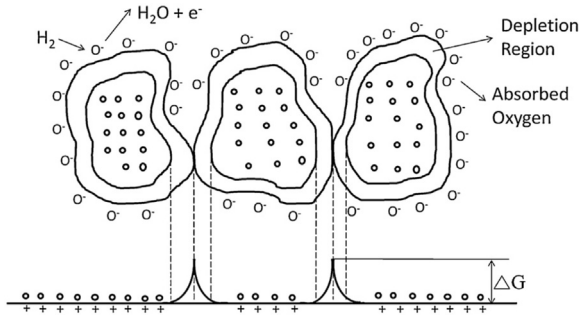

Fig. 10. Schematic diagram representing the gas sensing mechanism of AGZO NSs based sensor.

atmosphere and thereby captured electrons from the conduction band. This allowed the formation of three types of chemisorbed oxygen anions. Takata et al. [34] reported the formation of stable O^{2-} ions below 100 °C, O^{2-} ions between 100 and 300 °C, and O^{2-} ions above 300 °C. The resistivity of the sensing material was increased irrespective of temperature variation. It was argued that the adsorbed oxygen ions on the AGZO NSs based film surface subsisted in the form of O_2^- and O^-. In the absence of H_2 gas, the temperature dependent chemical reactions on the surface of NSs based film can be described as [35]:

$$O_2\,(gas) \leftrightarrow O_{2(ads)} \underset{T \le 100}{\longleftrightarrow} O_{2(ads)} + e^- \underset{T \le 100}{\longleftrightarrow} O^-_{2(ads)} \quad (7)$$

$$O_2\,(gas) \leftrightarrow O_{2(ads)} \underset{100 < T \le 300}{\longleftrightarrow} O_{2(ads)} + 2\,e^- \underset{100 < T \le 300}{\longleftrightarrow} O^-_{(ads)} \quad (8)$$

Upon exposing the sensor surface to H_2 gas, a reaction occurred between H atom and the adsorbed oxygen ions on the AGZO film surface which produced water vapor. Consequently, the amount of surface O^{-2} and O^- ions were reduced. Meanwhile, due to the transition of electrons to the conduction band the resistance of the film was dropped. In the presence of H_2 gas, the temperature dependent (low and high) chemical reactions can be depicted as:

$$2H_2 + O^-_{2(ZnO)} \underset{T \le 100}{\overset{\text{At } O_2 \text{ sites of ZnO}}{\longleftrightarrow}} H_2O_{(gas)} + e^- \quad (9)$$

$$2H_2 + O_2^-{}_{(ads)} \underset{100 < T \le 300}{\longleftrightarrow} H_2O_{(gas)} + e^- \quad (10)$$

$$2H_2 + O^-_{(ads)} \longleftrightarrow H_2O_{(gas)} + e^- \quad (11)$$

These reactions explain the adsorption-desorption mechanism assisted changes in the AGZO film resistivity as observed. The conductivity (sensitivity) of the n-type ZnO material was altered from low (absence of H_2) to high (presence of H_2). It was also reported in the literature that the sensitivity of such sensor could decrease with the increase of relative humidity [36]. Although to remove the physisorbed water low temperatures are needed but the strong chemisorption process of water onto AGZO (oxide) surface require high temperatures to eliminate the moisture [37]. In this work, the observed steady increase in the sensitivity with the raise of temperature indicated an insignificant influence of water on the sensor's sensitivity. Thus, it was asserted that the presence of hydroxyl ion and water on the AGZO NSs based film surface did not influence the sensor's sensitivity. This observation was attributed to the negligible diffusion of water molecules into the longer ZnO NSs [38]. Actually, the high aspect ratio and density of AGZO NSs could considerably reduce the negative effects moisture/humidity on the NSs surface (Table 3).

All the measurements were performed under identical conditions (temperature, concentration of oxygen inside the test chamber and the applied voltage (3 V) on the test sample). The oxygen molecules inside

Table 3
Selectivity of CO vs H_2 and CH_4 vs H_2 at operation temperature T = 100 °C.

Operation Temperature	Selectivity	
	CH_4 vs H_2	CO Vs H_2
100	0 2.031	1.656

test chamber were resulted from the adsorbed atmospheric oxygen on the AGZO NSs surface. The study aimed to detect the low concentrations of hydrogen gas (1250 ppm) due to its explosive nature. According to the chamber volume and the mask area, a thin layer of silver (Ag) of 250 nm with thick was deposited on the AGZO film via vacuum thermal evaporation method. Two planar Ag electrodes with gap area of 2 cm × 2 cm were fabricated on the film top.

The Al doping predominantly affected the sensing process at lower

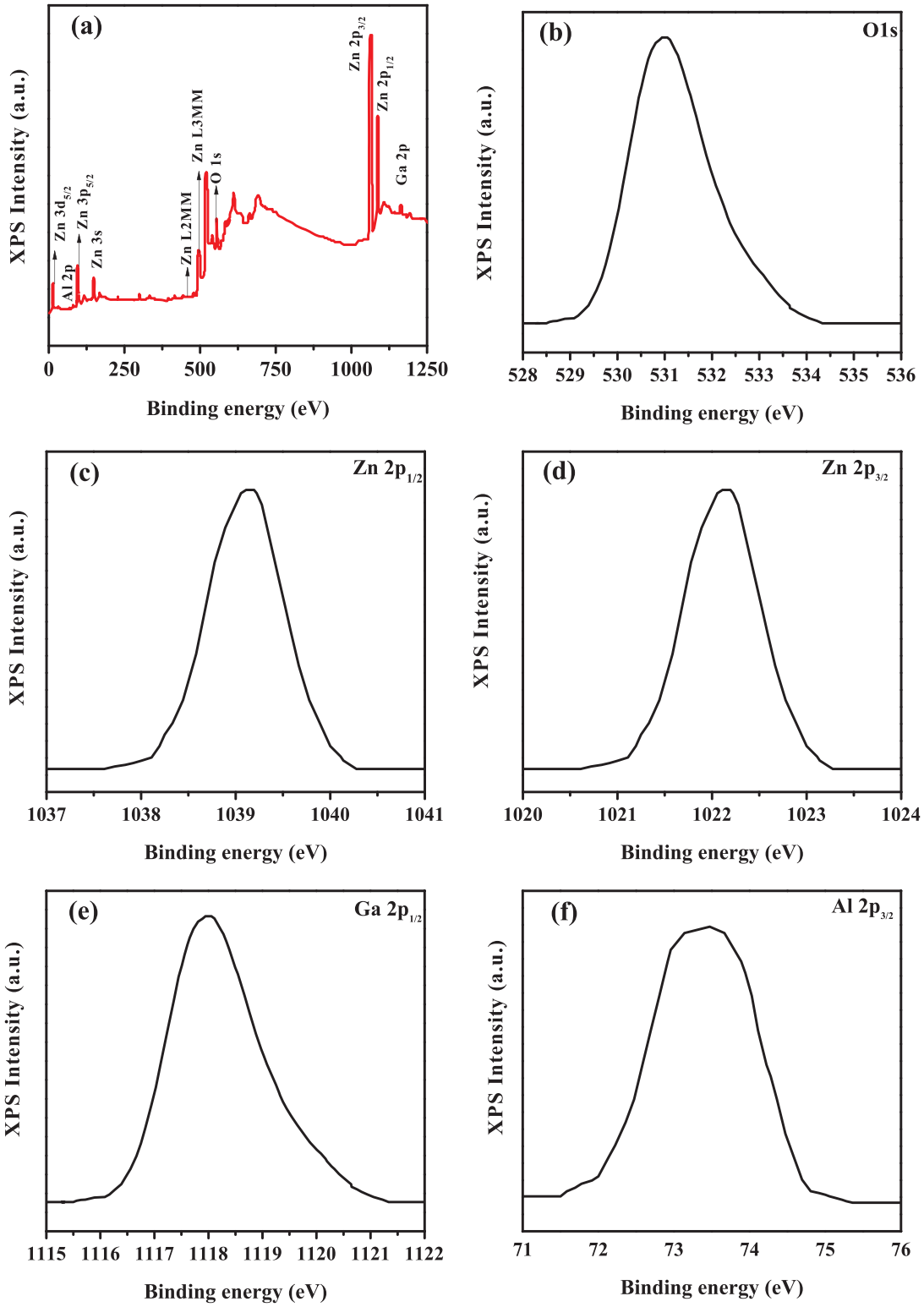

Fig. 11. XPS spectrum for the AGZO NSs (a), O 1s (b), Zn $2p_{1/2}$ (c), Zn $2p_{3/2}$ (d), Ga $2p_{1/2}$ (e) and (f) Al $2p_{3/2}$.

working temperature, while the actual semiconductor characteristic prevailed at higher working temperature. Therefore, the difference in the resistance value between high and low temperature was directly related to the Al-doping content and the carrier concentration or the quantity of Kroger–Vink defects originated from the Al-doping. Actually, the influencing mechanism of Al doping on the hydrogen sensing properties of AGZO is very complex. Al doping has significant effects on the AGZO crystal growth and its conductivity, which can directly affect the ZnO ethanol sensing property. Additionally, Al doping can change the AGZO acid–base characteristics and hence its gas sensing capacity [39]. Furthermore, Ga doping can strongly influence the sensor response by enlarging the AGZO surface area. Thus, surface area increase due to the reduction in the average crystallites size is not the main factor in improving the sensitivity of the GZO sensor [40].

Selectivity being a significant feature of the gas sensors can be defined as the capability to discriminate the analyte gases, which is expressed as [41]:

$$\text{Selectivity} = \text{sensitivity (gas A)/Sensitivity (gas B)} \quad (12)$$

where gas A is CH_4 or CO and gas B is H_2

To examine the AGZO NSs selectivity towards particular gases, these gas sensors sensitivities were compared at the same sensing temperature. The AGZO NSs selectivity for three different gases (H_2, CO and CH_4) were evaluated (Figs. 6(a), 8 and 9 respectively) at the operation temperature of 100 °C. It was found that CH_4 and CO gases exhibited higher sensitivity than H_2 gas at the same concentration. This was further illustrated by calculating the selectivity for CH_4 to H_2 gas (2.031) and CO to H_2 gas (1.656). Thus, AGZO NSs based gas sensors could effectively differentiate the hydrogen gas from other gases at 100 °C. This is essential where most sensor applications occur in ambient air conditions, where humidity shows the variation.

Fig. 11 illustrates the XPS profile of the optimum AGZO film (Al of 1 at% and Ga of 3 at%). It consisted of two peaks at the binding energy of 74.2 and 1118.1 eV, which were indexed as Al 2p3/2 and Ga 2p3/2, respectively. These peaks were allocated to the presence of Al-O and Ga-O bonding in the ZnO phase [42,43]. The ionic radius of Al^{3+}, Ga^{3+} and Zn^{2+} are 0.54, 0.62 and 0.74 Å and the bond lengths of Al-O, Ga-O and Zn-O are 2.70, 1.92 and 1.97 Å, respectively [44,45]. This clearly demonstrates that the integration of Ga with ZnO has a tendency to spur a smaller lattice deformation than that of Al.

4. Conclusion

A combined sol-gel and spin coating method was used to prepare pure Al/Ga co-doped ZnO film on p-type silicon substrate. The synthesized optimum AGZO films (1 at% of Al and 3 at% of Ga) containing vertically aligned nanorods were further used to fabricate some gas sensor. Optimum AGZO NSs film was characterized to determine the structure, morphology, and electrical properties. Hydrogen gas sensing performance of the designed AGZO NSs based sensor was evaluated. Besides, the selectivity of the AGZO NSs for three different gases such as H_2, CO and CH_4 were quantified. XRD pattern confirmed the high polycrystallinity of the AGZO film in the presence of ZnO wurtzite structure. The AGZO film revealed very low resistivity ($0.647 \times 10^{-2}\ \Omega$ cm) and high Hall mobility (7.667 cm^2/V s). The sensing attribute of the designed AGZO NSs based film sensor was determined at 100 and 125 °C by exposing it with hydrogen gas at varying concentrations (250, 500, 1250 and 1750 ppm). The gas sensing efficiency (sensitivity, response and recovery time) of the AGZO nanofilm based sensor was enhanced with temperature and H_2 gas concentration.

Acknowledgments

The project was supported by the Malaysian Ministry of Education for providing the financial assistance through PRGS vote 4L671 and FRGS 4F543. Thanks are also address to the Higher Education and scientific research of Iraq and University Of Al-Qadisiyah for providing Ph.D. study leave to Mr Hayder J. Al-Asedy.

References

[1] X.L. Chen, J.M. Liu, J. Ni, Y. Zhao, X.D. Zhang, Wide-spectrum Mg and Ga co-doped ZnO TCO thin films for solar cells grown via magnetron sputtering with H_2 introduction, Appl. Surf. Sci. 328 (2015) 193–197.
[2] J.H. Park, Y.C. Cho, J.M. Shin, S. Cha, C.R. Cho, H.S. Kim, S.J. Yoon, S. Jeong, S.E. Park, A. Lim, A study of transparent conductive aluminum-doped zinc oxide fabricated on a flexible polyethersulphone (PES) substrate, J.-Korean Phys. Soc. 51 (2007) 1968.
[3] W. Li, Y. Li, G. Du, N. Chen, S. Liu, S. Wang, H. Huang, C. Lu, X. Niu, Enhanced electrical and optical properties of boron-doped ZnO films grown by low pressure chemical vapor deposition for amorphous silicon solar cells, Ceram. Int. 42 (2016) 1361–1365.
[4] A.S. Enigochitra, P. Perumal, C. Sanjeeviraja, D. Deivamani, M. Boomashri, Influence of substrate temperature on structural and optical properties of ZnO thin films prepared by cost-effective chemical spray pyrolysis technique, Superlattices Microstruct. 90 (2016) 313–320.
[5] L. Zhang, J. Huang, J. Yang, K. Tang, B. Ren, Y. Hu, Y.L. Wang, L. Wang, The effects of thickness on properties of B and Ga co-doped ZnO films grown by magnetron sputtering, Mater. Sci. Semicond. Process. 42 (2016) (2016) 277–282.
[6] S.L. Ou, H.R. Liu, S.Y. Wang, D.S. Wuu, Co-doped ZnO dilute magnetic semiconductor thin films by pulsed laser deposition: excellent transmittance, low resistivity and high mobility, J. Alloy. Compd. 663 (2016) 107–115.
[7] T. Yan, C.Y. Lu, R. Schuber, L. Chang, D.M. Schaadt, M.M.C. Chou, K.H. Ploog, C.M. Chiang, Growth of c-plane ZnO on γ-$LiAlO_2$ (100) substrate with a GaN buffer layer by plasma assisted molecular beam epitaxy, Appl. Surf. Sci. 35 (2015) 824–830.
[8] H. Aydın, C. Aydın, A.A. Al-Ghamdi, W.A. Farooq, F. Yakuphanoglu, Refractive index dispersion properties of Cr-doped ZnO thin films by sol–gel spin coating method, Opt.-Int. J. Light Electron Opt. 127 (2016) 1879–1883.
[9] L. Duan, X. Zhao, Y. Wang, H. Shen, W. Geng, F. Zhang, Influence of Cd doping on structural and optical properties of (Cd, Al)-codoped ZnO powders synthesized via sol–gel method, J. Alloy. Compd. 645 (2015) 529–534.
[10] K. Zhu, Y. Yang, W. Song, Effects of substrate temperature on the structural, morphological, electrical and optical properties of Al and Ga co-doped ZnO thin films grown by DC magnetron sputtering, Mater. Lett. 145 (2015) 279–282.
[11] R. Ebrahimifard, M.R. Golobostanfard, H. Abdizadeh, Sol–gel derived Al and Ga co-doped ZnO thin films: an optoelectronic study, Appl. Surf. Sci. 290 (2014) 252–259.
[12] Y.N. Ahn, H. Yoon, S.H. Lee, H.H. Lee, H. Kim, Formation of randomly dispersed pores in Ga-doped ZnO between Al_2O_3 and glass via promoted atomic diffusion: experimental and computational study, Mater. Des. 93 (2016) 304–310.
[13] M.H. Mamat, M.Z. Sahdan, Z. Khusaimi, A.Z. Ahmed, A. Abdullah, M. Rusop, Influence of doping concentrations on the aluminum doped zinc oxide thin films properties for ultraviolet photoconductive sensor applications, Opt. Mater. 32 (2010) 696–699.
[14] M. Vishwas, K.N. Rao, A.R. Phani, K.A. Gowda, R.P.S. Chakradhar, Optical, electrical and structural characterization of ZnO: Al thin films prepared by a low cost sol–gel method, Solid State Commun. 152 (2012) 324–327.
[15] W. Lee, S. Shin, D.R. Jung, J. Kim, C. Nahm, T. Moon, B. Park, Investigation of electronic and optical properties in Al− Ga codoped ZnO thin films, Curr. Appl. Phys. 12 (2012) 628–631.
[16] J.P. Kim, J.S. Bae, T.E. Hong, M.S. Won, J.H. Yoon, B.S. Lee, H.J. Lee, Optical and electrical properties of ZnO films, codoped with Al and Ga deposited at room temperature by an RF sputtering method, Thin Solid Films 518 (2010) 6179–6183.
[17] F.J. Serrao, K.M. Sandeep, S. Bhat, S.M. Dharmaprakash, Sol-gel derived Al-Ga co-doped transparent conducting oxide ZnO thin films, AIP Conf. Proc. 1731 (2016) 80047.
[18] Y. Hou, A.M. Soleimanpour, A.H. Jayatissa, Low resistive aluminum doped nanocrystalline zinc oxide for reducing gas sensor application via sol–gel process, Sens. Actuators B: Chem. 177 (2013) 761–769.
[19] C. Takai-Yamashita, T. Ishino, M. Fuji, K. Inoue, Preparation and formation mechanism of ZnO supported hollow SiO_2 nanoparticle by an interfacial reaction through micropores, Colloids Surf. A: Physicochem. Eng. Asp. 493 (2016) 9–17.
[20] M. Isshiki, P. Sichanugrist, Y. Abe, T. Oyama, H. Odaka, M. Konagai, New method to measure whole-wavelength transmittance of TCO substrates for thin-film silicon solar cells, Curr. Appl. Phys. 14 (2014) 1813–1818.
[21] S. Zare, A.A. Ati, S. Dabagh, R.M. Rosnan, Z. Othaman, Synthesis, structural and magnetic behavior studies of Zn–Al substituted cobalt ferrite nanoparticles, J. Mol. Struct. 1089 (2015) 25–31.
[22] A. Henni, M. Abdellah, T. Laid, K. Amina, Studies on the structural, morphological, optical and electrical properties of Al-doped ZnO nanostructures prepared by electrochemical deposition, J. Electroanal. Chem. 763 (2016) 149–154.
[23] R. Al Asmar, S. Juillaguet, M. Ramonda, A. Giani, P. Combette, A. Khoury, A. Foucaran, Fabrication and characterization of high quality undoped and Ga_2O_3-doped ZnO thin films by reactive electron beam co-evaporation technique, J. Cryst. Growth 275 (2005) 512–520.
[24] M.A. Gondal, Q.A. Drmosh, Z.H. Yamani, T.A. Saleh, Synthesis of ZnO_2 nanoparticles by laser ablation in liquid and their annealing transformation into ZnO nanoparticles, Appl. Surf. Sci. 256 (2009) 298–304.
[25] D. Behera, B.S. Acharya, Nano-star formation in Al-doped ZnO thin film deposited by dip-dry method and its characterization using atomic force microscopy, electron

probe microscopy, photoluminescence and laser Raman spectroscopy, J. Lumin. 128 (2008) 1577–1586.
[26] D.W. Kang, S.J. Kim, T.H. Moon, H.M. Lee, M.K. Han, Effect of Ga doping on transparent and conductive Al-doped ZnO films prepared using magnetron co-sputtering, Jpn. J. Appl. Phys. 49 (2010) 125801.
[27] B. Houng, C.S. Hsi, B.Y. Hou, S.L. Fu, Fabrication and properties evaluation of aluminum and ruthenium co-doped zinc oxide thin films, J. Alloy. Compd. 456 (2008) 64–71.
[28] K.H. Ri, Y. Wang, W.L. Zhou, J.X. Gao, X.J. Wang, J. Yu, The structural properties of Al doped ZnO films depending on the thickness and their effect on the electrical properties, Appl. Surf. Sci. 258 (2011) 1283–1289.
[29] Z. Zhang, C. Bao, W. Yao, S. Ma, L. Zhang, S. Hou, Influence of deposition temperature on the crystallinity of Al-doped ZnO thin films at glass substrates prepared by RF magnetron sputtering method, Superlattices Microstruct. 49 (2011) 644–653.
[30] N. Yamazoe, J. Fuchigami, M. Kishikawa, T. Seiyama, Interactions of tin oxide surface with O_2, H_2O and H_2, Surf. Sci. 86 (1979) 335–344.
[31] L. Zhang, J. Zhao, H. Lu, L. Gong, L. Li, J. Zheng, H. Li, Z. Zhu, High sensitive and selective formaldehyde sensors based on nanoparticle-assembled ZnO micro-octahedrons synthesized by homogeneous precipitation method, Sens. Actuators B: Chem. 160 (2011) 364–370.
[32] X. Song, Z. Wang, Y. Liu, C. Wang, L. Li, A highly sensitive ethanol sensor based on mesoporous ZnO–SnO_2 nanofibers, Nanotechnology 20 (2009) (2009) 075501.
[33] P.T. Moseley, J.O. Norris, D.E. Williams, Techniques and Mechanisms in Gas Sensing, Adam Hilger, 1991.
[34] M. Takata, D. Tsubone, H. Yanagida, Dependence of electrical conductivity of ZnO on degree of sintering, J. Am. Ceram. Soc. 59 (1976) 4–8.
[35] O. Lupan, G. Chai, L. Chow, Novel hydrogen gas sensor based on single ZnO nanorod, Microelectron. Eng. 85 (2008) 2220–2225.
[36] W. Widanarto, C. Senft, O. Senftleben, W. Hansch, I. Eisele, Characterization and sensing properties of ZnO film in FG-FET sensor system for NO_2 detection, Int. J. Basic Appl. Sci. IJBAS-IJENS 11 (2011) 104–108.
[37] K. Scharnagl, M. Eriksson, A. Karthigeyan, M. Burgmair, M. Zimmer, I. Eisele, Hydrogen detection at high concentrations with stabilised palladium, Sens. Actuators B: Chem. 78 (2001) 138–143.
[38] S.M. Mohammad, Z. Hassan, R.A. Talib, N.M. Ahmed, M.A. Al-Azawi, N.M. Abd-Alghafour, C.W. Chin, N.H. Al-Hardan, Fabrication of a highly flexible low-cost H_2 gas sensor using ZnO nanorods grown on an ultra-thin nylon substrate, J. Mater. Sci.: Mater. Electron. 27 (2016) 9461–9469.
[39] Z. Yang, Y. Huang, G. Chen, Z. Guo, S. Cheng, S. Huang, Ethanol gas sensor based on Al-doped ZnO nanomaterial with many gas diffusing channels, Sens. Actuators B: Chem. 140 (2009) 549–556.
[40] M. Hjiri, R. Dhahri, L. El Mir, S.G. Leonardi, G. Neri, Excellent CO gas sensor based on Ga-doped ZnO nanoparticles, J. Mater. Sci.: Mater. Electron. 26 (2015) 6020–6024.
[41] N. Yamazoe, G. Sakai, K. Shimanoe, Oxide semiconductor gas sensors, Catal. Surv. Asia 7 (2003) 63–75.
[42] D.K. Kim, H.B. Kim, Room temperature deposition of Al-doped ZnO thin films on glass by RF magnetron sputtering under different Ar gas pressure, J. Alloy. Compd. 509 (2011) 421–425.
[43] F. Mitsugi, Y. Umeda, N. Sakai, T. Ikegami, Uniformity of gallium doped zinc oxide thin film prepared by pulsed laser deposition, Thin Solid Films 518 (2010) 6334–6338.
[44] M.C. Jun, S.U. Park, J.H. Koh, Comparative studies of Al-doped ZnO and Ga-doped ZnO transparent conducting oxide thin films, Nanoscale Res. Lett. 7 (2012) 639.
[45] Z. Yang, D.C. Look, J.L. Liu, Ga-related photoluminescence lines in Ga-doped ZnO grown by plasma-assisted molecular-beam epitaxy, Appl. Phys. Lett. 94 (2009) 072101.